

A GUIDE TO THE BOTT INDEX AND LOCALIZER INDEX

TERRY A. LORING

ABSTRACT. The Bott index is inherently global. The pseudospectral index is inherently local, and so now the preferred name is the localizer index. We look at these on a rather standard model for a Chern insulator, with an emphasis how to program these effectively. We also discuss how to tune the localizer index so it behaves like a global index.

CONTENTS

1. Introduction	1
2. The Clifford spectrum	2
3. Formulas for the Bott index	6
4. Extending an old study	8
5. The localizer index	11
6. Localizer index goes global	19
7. Local nature of the localizer	22
Acknowledgments	24
References	24

1. INTRODUCTION

The most elegant real-space topological invariant to describe a Chern insulator is computed on an infinite model, the index of a Fredholm operator:

$$(1.1) \quad \text{ind} \left(P \frac{X + iY}{|X + iY|} P + I - P \right).$$

Here X and Y represent position operators and P is the Fermi projection derived via functional calculus from the Hamiltonian H . This does not require translation invariance, just a gap in the spectrum of H containing the Fermi level. By the work of Bellissard, van Elst, and Schulz-Baldes [5] we know this equals the Chern number in the case of translation invariant systems.

For numerical studies we must work with finite matrices. This can be done in several ways. Some infinite area formulas can be approximated by finite area calculations. For example, Prodan explains in [30, §6] how a finite area approximation leads to a number that, while not an integer, converges rapidly to the noncommutative Chern number. Kitaev [19, §C.3] defined a generalized notion of the Chern number with a formula to be computed over an infinite area. Several authors have noted that in many instances a finite-area approximation converges well to Kitaev's generalized Chern number [8, 29]. This method has the advantage of giving a local index. Thus two lattice models can be melded on a linear interface and a

Key words and phrases. Chern insulator, numerical linear algebra, Bott index, K -theory.

local (non-integral) real-space marker can be defined that seems to sensibly mark topological and trivial areas [29, Figure 4.d].

An alternate approach is to define, via K -theory, an integer associated to a finite model, and attempt to prove that this integer coincides with the infinite-area index in (1.1). The C^* -algebra in this case is typically very elementary, just the n -by- n complex matrices $\mathbf{M}_n(\mathbb{C})$. In proving things about such an index, one tends to need complicated C^* -algebras defined by generators and relations [9, 12] and tools like E -theory [10]. Keeping the definitions simple should, in general, lead to fast algorithms.

The essence of this approach is to look to the old theory of what K -theory can tell us about almost commuting matrices [22, 12]. For example of what was known by the 1990s, consider two unitary matrices that almost commute. These are sometimes small perturbations of commuting unitary matrices, sometimes not. It can be shown [13, Theorem 6.14] that being close or far from commuting unitary matrices can be inferred from the value of a K -theoretic invariant. There are ways to compute this invariant that do not really look like K -theory [14], and other formulas that are straight-forward computations involving formulas for idempotents. Indeed, there are many, many formulas we might choose [12].

Finite models force upon us a choice of boundary conditions. Actually, first one selects a shape, with square being the *de facto* choice. A frequent choice in physics is to use periodic boundary conditions, which implicitly turns the square into a torus. This is great mathematically, being an enabler of the Fourier transform. However, this choice eliminates edge modes, arguably the most attractive feature of a Chern insulator. The other choice is working with open boundaries, where on a lattice model the hopping terms in the infinite-area Hamiltonian are dropped if they involve sites outside the finite patch. Mathematically, this is just the obvious compression of the infinite-area Hamiltonian. This leads to edge modes in the finite model, and is more realistic than a torus model. This is actually an annoyance in some instances, as the edge modes can make it harder to see bulk phenomenon in a small system [25].

2. THE CLIFFORD SPECTRUM

The Clifford spectrum gives a nice way to see the difference between the Bott index and the localizer index. In both cases there is a topological space associated to a finite system, but the spaces are very different. All sorts of spaces can emerge as the Clifford spectrum of a finite collection of Hermitian matrices. This is well established in string theory, for example in [7, 31]. Kisil [18] observed earlier that the joint spectrum of a few Hermitian matrices could be a surface.

For a periodic system, square with sides of length L , one cannot easily work with the position operators X and Y as these will have commutator norm with the Hamiltonian H on the order of L . Thus one considers “periodic observables”

$$U = e^{\frac{2\pi i}{L}X}, \quad V = e^{\frac{2\pi i}{L}Y}$$

which really correspond to four observables (Hermitian matrices)

$$M_1 = \cos\left(\frac{2\pi i}{L}X\right), \quad M_2 = \sin\left(\frac{2\pi i}{L}X\right), \quad M_3 = \cos\left(\frac{2\pi i}{L}Y\right), \quad M_4 = \sin\left(\frac{2\pi i}{L}Y\right).$$

One has then a fifth matrix

$$M_5 = P$$

where P is the spectral projection for H associated to energy levels below the Fermi gap.

The Clifford spectrum of Hermitian matrices M_1, \dots, M_d (all of the same size) is a subset $\Lambda(M_1, \dots, M_d)$ of \mathbb{R}^d , defined as follows. One chooses nontrivial $\Gamma_1, \dots, \Gamma_d$ that form a Clifford representation, here meaning

$$\Gamma_j^\dagger = \Gamma_j, \quad \Gamma_j^2 = I$$

for all j and

$$\Gamma_j \Gamma_k = -\Gamma_k \Gamma_j$$

whenever $j \neq k$. Then one forms the *localizer*

$$L_\lambda(M_1, \dots, M_d) = \sum (M_j - \lambda_j) \otimes \Gamma_j$$

(called sometimes the localized Dirac operator [31]). Then

$$\lambda \in \Lambda(M_1, \dots, M_d) \iff L_\lambda(M_1, \dots, M_d) \text{ is singular}$$

defines the Clifford spectrum of (M_1, \dots, M_d) , and this is independent of the choice of Γ_j .

For reasonable H (one needs some locality, boundedness and a reasonable gap) when L is large enough, we have U, V and P that satisfy the following:

$$(2.1) \quad \begin{aligned} U^\dagger U &\approx I, & UU^\dagger &\approx I, & V^\dagger V &\approx I, & VV^\dagger &\approx I, \\ UV &= VU, & UP &\approx PU, & VP &\approx PV, \\ P^2 &= P, & P^\dagger &= P. \end{aligned}$$

All this can be made ever so rigorous, as in [23]. What is critical is that if these relations were exact, they would become equations in \mathbb{R}^5 that define a copy of the space

$$\mathbb{T} \sqcup \mathbb{T},$$

meaning two disjoint copies of the torus.

What we have then is a fuzzy version of two copies of the torus, and the Clifford spectrum will be a subset of \mathbb{R}^5 that is close to the union of two tori. It is the topology of $\mathbb{T} \sqcup \mathbb{T}$ that is used in defining the Bott index. Perhaps, when the Bott index is nonzero, and in a clean system on a regular lattice, the Clifford spectrum of M_1, \dots, M_5 is homeomorphic to $\mathbb{T} \sqcup \mathbb{T}$. Proving this is out of reach, for now.

The localizer index is based on different topology, and it starts with open boundaries. In this case, H will almost commute with $X_0 = \frac{2}{L}X$ and $Y_0 = \frac{2}{L}Y$. Notice *we cannot expect a gap in the spectrum of H* . One can spectrally flatten the infinite-area Hamiltonian and compress that, but the result will still be ungapped due to edge modes.

Let us assume the system is centered at 0. The Clifford spectrum of (X_0, Y_0, H) will be some compact subset of \mathbb{R}^3 . The key relation here is

$$L_0(X_0, Y_0, P) \geq c,$$

where $c > 0$ is roughly that spectral gap in the infinite area Hamiltonian. See [27] for details on what we know about c . We also have relations

$$(2.2) \quad \begin{aligned} -1 &\leq X_0 \leq 1, & -1 &\leq Y_0 \leq 1, \\ X_0 Y_0 &= Y_0 X_0, & X_0 H &\approx H X_0, & Y_0 H &\approx H Y_0, \\ -C &\leq H \leq C \end{aligned}$$

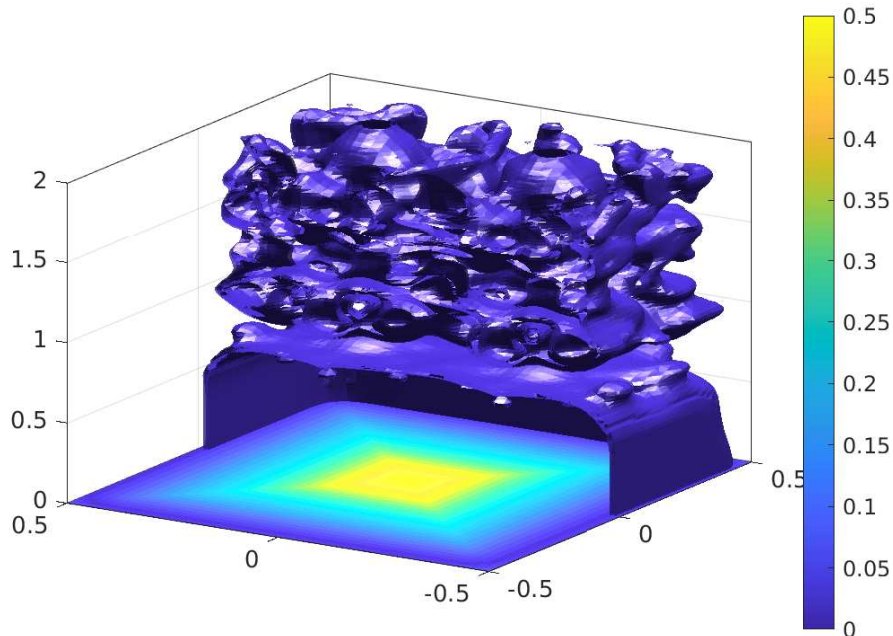


FIGURE 2.1. Some of the pseudospectrum of a round Chern insulator. Along the x-y plane the gap $\|L_\lambda(X_0, Y_0, H)^{-1}\|^{-1}$ is indicated by color. Also shown are portions of some contour surfaces for a few gap sizes very close to zero.

where C is the norm of the infinite-area Hamiltonian. We have here a fuzzy version of

$$S(C, c) = ([-1, 1] \times [-1, 1] \times [-C, C]) \setminus B(c)$$

where $B(c)$ is the open ball of radius c at the origin. The pseudospectrum $\Lambda(X_0, Y_0, H)$ is expected to be some manner of a surface within $S(C, c)$. While $S(C, c)$ is homotopic to a sphere, the space $\Lambda(X_0, Y_0, H)$ will be more complicated, and is very difficult to compute. Still, it will have a K -theory class coming ultimately from the K -theory of the sphere which will lead to the localizer index.

If one uses the spectrally flattened infinite-area Hamiltonian and compresses that to the finite square system, one has then a Hamiltonian H_1 that has “spectrum localized near $(0, 0)$ equal to a fuzzy $\{0, 1\}$ ” in the sense put forward in [25]. A naive expectation is that the Clifford spectrum of (X_0, Y_0, H_1) will be roughly two copies of the square. In the case of trivial insulators, this is what one should to find. It is the edge states, when the system is topological, that work to glue together the top and bottom square to create more of a cube. This is all heuristic, until we find better ways to compute the Clifford spectrum. In the case of the Bott index, the periodic boundary conditions turn the top and bottom square each into a torus. In the case of the localizer index, when the system is topologically non-trivial, the edge states add to the Clifford spectrum, forming walls that join the top and bottom squares into something like a sphere.

We can, with lots of computer time, compute the Clifford pseudospectrum of (X_0, Y_0, H) . This is essentially a blurred out version of the Clifford spectrum, and formally is the scalar-valued map on 3-space

$$\lambda \mapsto \|L_\lambda(X_0, Y_0, H)^{-1}\|^{-1}.$$

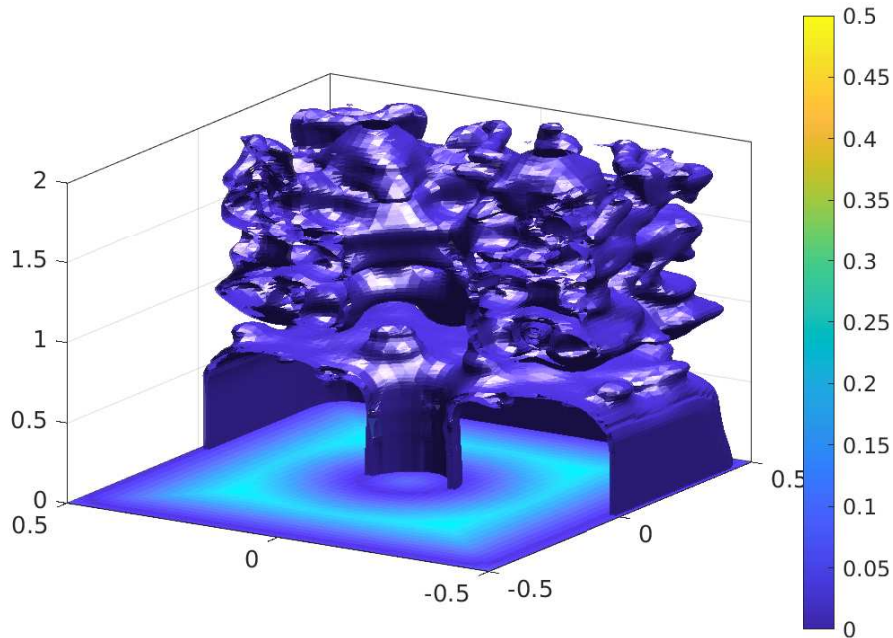


FIGURE 2.2. Some of the pseudospectrum of a round Chern insulator with a hole in it.

Where this is zero is the Clifford spectrum. We can more easily compute where this is small, and get an estimate on where lives the Clifford spectrum.

Now that we are working with just three observables, we can specify a choice for the Γ_j , specifically $\Gamma_1 = \sigma_x$, $\Gamma_2 = \sigma_y$, $\Gamma_3 = \sigma_z$. Then

$$(2.3) \quad L_\lambda(M_1, M_2, M_3) = (M_1 - \lambda_1) \otimes \sigma_x + (M_2 - \lambda_2) \otimes \sigma_y + (M_3 - \lambda_3) \otimes \sigma_z$$

so

$$L_\lambda(X_0, Y_0, H) = \begin{bmatrix} H - \lambda_3 & (X_0 - \lambda_1) - i(Y_0 - \lambda_2) \\ (X_0 - \lambda_1) + i(Y_0 - \lambda_2) & -H + \lambda_3 \end{bmatrix}.$$

Ideally, the reader would see this computed for the Hamiltonian considered in the rest of the paper. As the author has consumed already considerable resources from the Center for Advanced Research Computing at the university of New Mexico, it seems prudent to offer the reader a different example, which was computed earlier. Here the Hilbert space is built from a square sample of a quasilattice, and the Hamiltonian is a variation on a “ $p_x + ip_y$ ” tight binding model, as in [15, 25]. A portion of the pseudospectrum is indicated in Figure 2.1. The Hamiltonian is the compressed original Hamiltonian, not a compression of the spectrally flattened Hamiltonian. The pseudospectrum extends up to about $\lambda_3 = 6$ and down to about $\lambda_3 = -6$.

The localizer can have a very large gap even when the Hamiltonian does not. This happens because, by design, the localizer can focus on “bulk states” while ignoring edge states. This can happen even with strong disorder, as is illustrated by the disorder-averaged study in Section 6 and by the examination of the localizer spectrum in [33].

Unlike the Bott index, the localizer index is flexible in what geometry is used. For example, one can use a square with a disk cut out of the middle. In this case, there are additional edge modes and the result is more like a torus than a sphere. See Figure 2.2.

3. FORMULAS FOR THE BOTT INDEX

The first step in finding an invariant for matrices with the relations as in Equation 2.1 is to eliminate the second torus (the one at high energy). This is the step of considering band-compressed angular position operators

$$PUP : P(\mathbb{C}^n) \rightarrow P(\mathbb{C}^n)$$

and

$$PVP : P(\mathbb{C}^n) \rightarrow P(\mathbb{C}^n).$$

A more precise notation is $(PUP)|_{P\mathbb{C}^n}$ and $(PVP)|_{P\mathbb{C}^n}$. These are operators, not matrices. To obtain matrices we must select a basis for the range $P(\mathbb{C}^n)$ of P . Assuming one obtains the Fermi projector P by doing a full diagonalization of the Hamiltonian $H \in \mathbf{M}_n(\mathbb{C})$ such a basis is then available at no further cost.

This is a sticking point. Taking a full diagonalization of H forces us to work with dense matrices. As we are dealing with approximate relations, we could work with an approximation P_0 to P that is sparse. This is a standard procedure in quantum chemistry [6]. However, there are other parts to the Bott index formula where a sparse approach is not at all clear. Also, we need sparse approximate spectral flattening given only a mobility gap, which will be harder than the case of a true gap. For now, the Bott index is a dense matrix formula, which is its major limitation.

Suppose then that you have used an eigensolver on H to find for \mathbb{C}^n a basis $\mathbf{q}_1, \dots, \mathbf{q}_n$ of eigenvalues, with $\mathbf{q}_1, \dots, \mathbf{q}_m$ in the subspace below the Fermi level and $\mathbf{q}_{m+1}, \dots, \mathbf{q}_n$ above. (In a disordered system, there may be no apparent gap, but one still is selecting a Fermi level.) Then $\mathbf{q}_1, \dots, \mathbf{q}_m$ is a basis for $P(\mathbb{C}^n)$. The matrices, with respect to this basis, for the operators $(PUP)|_{P\mathbb{C}^n}$ and $(PVP)|_{P\mathbb{C}^n}$ are

$$(3.1) \quad U_1 = W^\dagger U W, \quad V_1 = W^\dagger V W,$$

where

$$W = \begin{bmatrix} | & & | \\ | & & | \\ \mathbf{q}_1 & \cdots & \mathbf{q}_m \\ | & & | \\ | & & | \end{bmatrix}.$$

Notice W is a partial isometry.

The smaller matrices U_1 and V_1 satisfy the more familiar relations

$$(3.2) \quad \boxed{\begin{aligned} U_1^\dagger U_1 \approx I, \quad U_1 U_1^\dagger \approx I, \quad V_1^\dagger V_1 \approx I, \quad V_1 V_1^\dagger \approx I, \\ U_1 V_1 \approx V_1 U_1 \end{aligned}}$$

There is a theory on how to create a K -theoretic index for such approximate relations [12]. Such an index is never unique. All we can say is that for very small commutators two such indices will agree. We can't usually say how small the commutator must be for two such invariants to agree. Some of these choices for invariants will make more sense physically than others. Some will be faster to compute than others.

The general method here starts with a formula for a projector-valued function on the torus, and 2-by-2 matrices suffice. For example

$$(3.3) \quad (w, z) \mapsto \begin{bmatrix} f(z) & g(z) + ih(z)w \\ g(z) - ih(z)w & 1 - f(z) \end{bmatrix}$$

for $|v| = |w| = 1$. In fact, this need not take values only in projectors: approximate projectors ($p^2 \approx p$) will be fine. Thus we assume $fg \approx 0$ and $f^2 + g^2 + h^2 \approx f$. The formulas used must make sense when applied to noncommuting, nonunitary matrices. For example, one can take f, g and h to be Laurant polynomials in z (so trig polynomials in the argument of z). Then the K -theoretic index is the number of eigenvalues above $\frac{1}{2}$, minus the number below, of the matrix

$$\begin{bmatrix} f(V_1) & g(V_1) + ih(V_1)U_1 \\ g(V_1) - iU_1^\dagger h(V_1) & 1 - f(V_1) \end{bmatrix}.$$

This is a simplified version of what was called the trig method in [26].

There are many variation possible on this. Moreover one can work directly with U, V and a sparse approximation P and use the theory of [12] for the space $\mathbb{T} \sqcup \mathbb{T}$. This might lead to faster algorithm than is available to the Bott index, in theory.

An issue with all invariants using this method is that they do not treat all parts of a square lattice equally. This is because the function in (3.3) is a continuous function from the torus to the Bloch sphere. Every such map has at least one point on the sphere where some nonzero area of the torus is smashed together sent to a region of zero area on the sphere.

In the special case of the approximate relations in Equation 3.2, there is an elegant alternative to produce indices proven equivalent (equal for small commutators) to an index as above. For the case of almost commuting unitary matrices, this was proven a while back [14]. The formula was modified to work for almost unitary matrices that almost commuting more recently [26]. It also treats U_1 and V_1 symmetrically, and treats all areas in the lattice equally (if the lattice is treated as on a torus). This alternate formula is what physicists now call the Bott index.

The Bott index uses the smaller matrices from Equation 3.1 and is

$$(3.4) \quad \text{Bott}(U, V, P) = \Re \left(\frac{1}{2\pi i} \text{Tr} \left(\log \left(U_1 V_1 U_1^\dagger V_1^\dagger \right) \right) \right)$$

where \Re indicates real part. It is guaranteed, in theory, to makes sense, and be in integer, when $(\infty, 0]$ is not in the spectrum of $U_1 V_1 U_1^\dagger V_1^\dagger$. In practice eigenvalues of $U_1 V_1 U_1^\dagger V_1^\dagger$ very near $(\infty, 0]$ also cause trouble. This formula uses the matrix logarithm, and *you don't want to compute a matrix logarithm* as that takes a long time.

Lemma 3.1. *If X is a matrix with no spectrum lying in the set $(-\infty, 0)$, then*

$$\Re \left(\frac{1}{2\pi i} \text{Tr}(\log(X)) \right) = \sum \Re \left(\frac{1}{2\pi i} \log \left(\frac{\lambda}{|\lambda|} \right) \right)$$

where $\lambda_1, \dots, \lambda_n$ are the eigenvalues of X listed according to multiplicity. In all instances the usual branch of \log is assumed.

Proof. This follows easily from the spectral mapping theorem for analytic functions. □

Notice we have no need for any eigenvectors of $DCD^\dagger C^\dagger$, just the list of eigenvalues. After multiplying matrices to form the commutator, you the calculate all the eigenvalues, take the

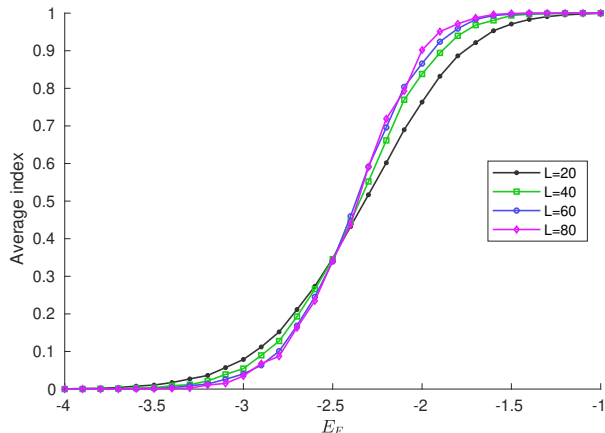


FIGURE 4.1. Bott index averaged over disorder as a function of the Fermi level: $L = 20$ (12,664 samples); $L = 40$ (7,681 samples); $L = 60$ (3,013 samples); $L = 80$ (1,121 samples).

scalar logarithm of each, and add those. The heart of the algorithm is as follows, when implemented in Matlab.

```

U = W'*exp_x*W;
V = W'*exp_y*W;
T = eig(commutator); % Just a list of eigenvalues
index = -sum(imag(log(T)))/(2*pi);
index = round(index);

```

Here W is the partial matrix of eigenvectors and \exp_x and \exp_y are the normalized exponentiation position matrices U and V . Also U and V are what have been denoted U_1 and V_1 . See the file `oldBottNoGap.m` in the supplementary files [3].

It could be that someone has computed the projector P onto the subspace of states below the gap, but not an orthonormal basis for that space. This will happen if you use the methods of quantum chemistry [6] to approximately compute the Fermi projector P . In that case, one can use the almost commuting matrices

$$(3.5) \quad A = PUP + (I - P) \text{ and } B = PVP + (I - P)$$

and it can be shown that

$$\text{Bott}(U, V, P) = \Re \left(\frac{1}{2\pi i} \text{Tr} (\log (BAB^\dagger A^\dagger)) \right).$$

Since A and B are larger than U_1 and V_1 then this may end up as the slower method, but perhaps someone knows how to compute the trace of the log of a sparse matrix quickly. Without a method to deal with that trace of a matrix log, one is advised to work only with U_1 and V_1 .

4. EXTENDING AN OLD STUDY

For the purposes of evaluating the algorithm of the Bott index, we replicate and extend the numerical study in [26] (see also [24]). The reason to select a known model Hamiltonian and disorder-induced transition is to keep the focus here on the methods for computing the Bott index.

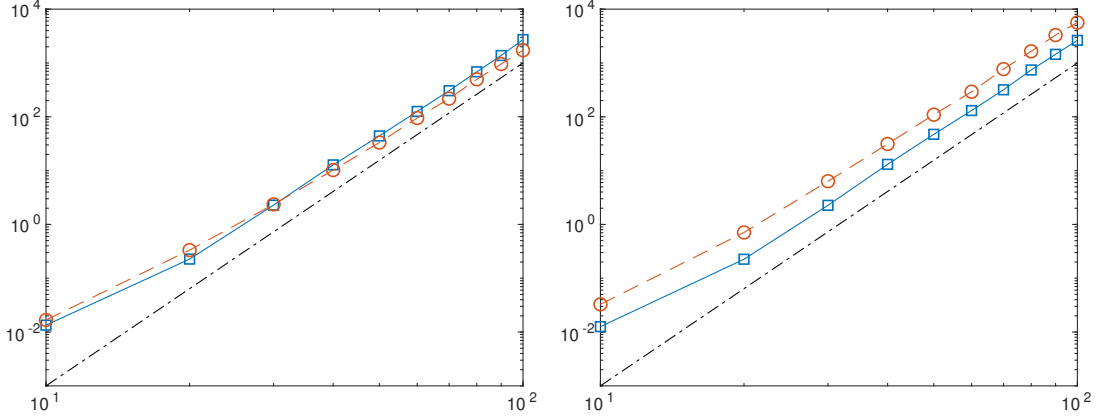


FIGURE 4.2. For $L = 10$ to $L = 100$ the average time. Left panel is the preferred method using the matrices as in equation 3.2, right panel the method using the larger matrices described in Equation 3.5. The solid line with squares indicates the time in seconds needed for a full diagonalization of the Hamiltonian. The dashed line indicates the time in seconds for the rest of the calculation, with the energy cutoff a bit below the Fermi level. The testing was performed on a 8-core computer with each core rated at 2.67GHz. For reference, the dotted line plots the curve $y = (10^{-9}) L^6$. These plots are based on computing one Bott index for each of 10 disordered Hamiltonians for each value of L .

We start with a regular square lattice, with periodic boundary conditions, with two basis elements at each site. Upon this we consider a real-space tight binding model, associating a Hamiltonian term to each site of the tiling and a hopping matrix to each link between closest neighboring sites. The on-site element corresponding to site j is

$$H_j = (M - 4B + W_j)I_2$$

where M and B are constants, and W_j varies by site, each W_j independently taken from a uniform distribution in $[-4, 4]$. The full hopping term between sites j and k , for j to the left of k is

$$H_{jk} = B\sigma_z + A\sigma_x$$

for j below k is

$$H_{jk} = B\sigma_z + A\sigma_y$$

The constants we will use are

$$A = 1, B = -1, C = 0, M = -2$$

which is as was done in producing [26, Fig. 1].

In other parts of [26] $M = -1$ was sometimes used. The meaning here of the constant A is off by $\frac{1}{2}$ how it is used in [17]. We continue to use the convention from [26] as listed above, and in any case the reader is encouraged to look at the file `ChernSystem.m` in the supplementary files [3] to see how the Hamiltonian and lattice are constructed.

As in [26] we vary the Fermi level for many Hamiltonians with different disorder terms. The index averaged over disorder that resulted is shown in Figure 4.1. The improvements in computing hardware over the past twelve years gave a moderate improvement, as now it is

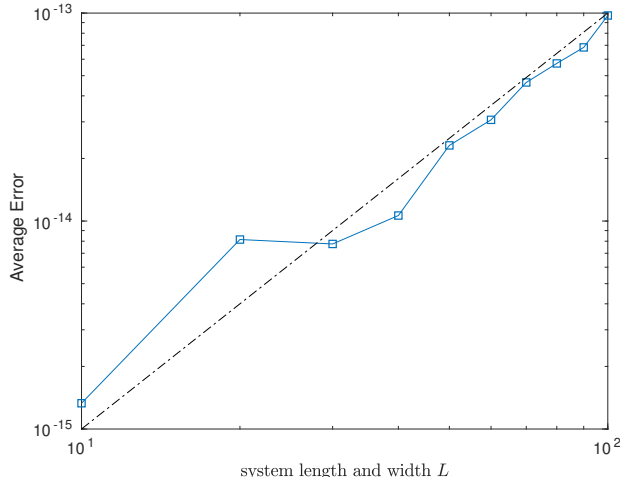


FIGURE 4.3. For $L = 10$ to to $L = 100$ the average error, defined as the distance to the closest integer. The solid line is the average error while, for reference, the dotted line plots the curve $y = (0.4 \times 10^{-17}) L^2$. This plot is based on 32 samples for each value of L .

feasible to work up to $L = 80$ instead of only $L = 60$, as in [26, Fig. 1]. Also, more samples were computed, so the resulting plots are clearer.

As we are computing all eigenvalues of some dense matrices, the time needed to compute the Bott index is expected to grow as the cube of system size, so $\mathcal{O}(L^6)$. Multiple values of the Bott index, for multiple Fermi levels, can be computed from the same diagonalization of the Hamiltonian, so in timing this algorithm it makes sense to time the Hamiltonian diagonalization separately from the time to compute a single Bott index given that diagonalization. As one can see from the left panel of Figure 4.2, both tasks do take time that grows in what looks like $\mathcal{O}(L^6)$.

As a comparison, the timing is reported (right panel of Figure 4.2) as well for the algorithm that uses the larger matrices of Equation 3.5. There is accumulated numerical error that keeps the result from being exactly an integer. This is generally ignored; one just rounds to the nearest integer. In Figure 4.3 is shown the distance to the nearest integer. This seems like it will be negligible even for systems so large that computing a single Bott index will be impractical.

It is worth pointing out that we do not, it seems, have a theory that tells us what the correct answer is here for the disordered averaged Bott index. However, the Bott index is known to correlate, in the gapped case, to the Kubo conductance [16, Lemma 5.6]. It has been used and evaluated in many settings, such as [11, 4, 32]. What Figure 4.3 is showing is that the computed Bott index come out very close to an integer, the error coming from the cumulative errors in calculating eigenvalues numerically.

The plot of the time needed makes it seem that computing a Bott index for a 100-by-100 system is reasonable. If computing an average over disorder, and at multiple Fermi levels, this is not the case, as the total time needed is excessive. On the other hand, since the number of samples needed decreases with system size, the growth in that case is more like $\mathcal{O}(L^5)$. That is still a problem, so if one wants to push this study further, one needs to be doing sparse matrix computations.

5. THE LOCALIZER INDEX

The localizer index works only with open boundaries. Unlike the Bott index, it can easily be modified for different symmetry classes and physical dimensions [24]. Here we focus on 2D system in class AI. Several papers [15] referred to this index as the pseudospectrum index, but that is misleading as the index is defined where the pseudospectrum isn't.

We have three observables (X, Y, H) with X and Y position and H the Hamiltonian. We could change units in X and Y and would still have three observables, now $(\kappa X, \kappa Y, H)$ for some nonzero, finite scaling constant κ . If λ is not in $\Lambda(\kappa X, \kappa Y, H)$ then the *localizer index at λ for $(\kappa X, \kappa Y, H)$* is

$$\frac{1}{2} \text{Sig}(L_\lambda(\kappa X, \kappa Y, H)),$$

where L_λ is the localizer of Equation 2.3 and $\text{Sig}(M)$ refers to the number of positive eigenvalues minus the number of negative eigenvalues of the nonsingular Hermitian matrix M .

In [24] the localizer was referred to as the Bott element since it does give a representative of the Bott element when applied to standard position coordinates on the sphere. Now that the Bott index is rather firmly entrenched in physics, it seems prudent to call it the localizer. This reflects the fact that one can use the localizer to differentiate edge from bulk states [25].

It is important to not compute all the positive or all the negative eigenvalues of the localizer when computing the index. That would defeat the advantage we gain from the fact that $L_\lambda(\kappa X, \kappa Y, H)$ should be a sparse matrix. One might need to zero-out small hopping terms between distant sites to ensure H is sparse. In general κX are κY are diagonal, and so very sparse.

If M is nonsingular and Hermitian, one computes an LDLT decomposition of M and uses Sylvester's law of inertial to compute the signature of M . This means, in practice, one finds a factorization

$$M = S^{-1} P L D L^\dagger P^\dagger S^{-1}$$

where S is diagonal with positive values on the diagonal, P is a permutation matrix, L is lower triangular, and D is block-diagonal, with both 1-by-1 and 2-by-2 blocks. Since

$$M = (S^{-1} P L) D (S^{-1} P L)^\dagger$$

we have

$$\text{Sig}(M) = \text{Sig}(D)$$

and the signature of D is the sum of the signatures of the blocks of D .

Unfortunately, we require LDLT for a sparse complex Hermitian matrices, while Matlab [1] and MUMPS [2] only allow for sparse real symmetric matrices. A workaround is based on the usual embedding

$$a + ib \mapsto \begin{bmatrix} a & b \\ -b & a \end{bmatrix}$$

of the reals into complex matrices. As such, one computes the signature of

$$\begin{bmatrix} \Re(M) & \Im(M) \\ -\Im(M) & \Re(M) \end{bmatrix}$$

and divides by two. See `signature.m` in the supplementary files [3].

Certainly the resulting algorithm seems fast. Figure 5.1 shows how the time to compute a single localizer index grows at a smaller order than the growth we saw for the Bott index. It is not so hard to compute a single localizer index for a system with $L \approx 1000$ [25]. However,

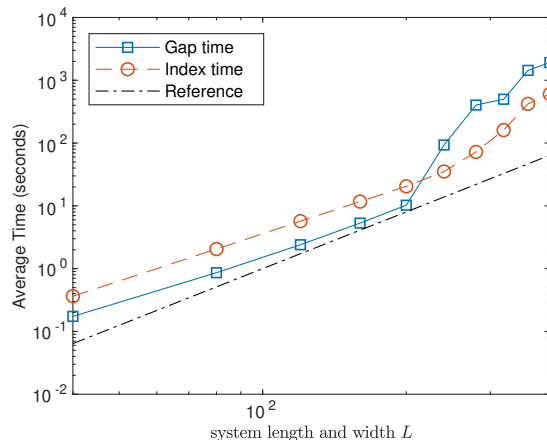


FIGURE 5.1. For $L = 40$ to $L = 400$ the average time for the localizer method, time to compute the gap and to compute the index plotted separately. The testing was performed on a 8-core computer with each core rated at 2.67GHz. For reference, the dotted line plots the curve $y = (5 \times 10^{-9}) L^4$. These plots are based one Fermi level of 10 disordered Hamiltonians for each value of L .

this is not a thorough analysis if we are looking at a disorder averaged index study. Open boundaries and periodic boundary conditions will have different effects for the same system size. Also, the localizer index is, at its heart, a local index. To see the effect of growing system size, we ought to be working with a global index. It is possible to make the localizer index behave globally, but this conversion is not trivial.

Unless we are dealing with a defect (like the hole in the system used in Figure 2.2) we are going to set (λ_1, λ_2) to $(0, 0)$, or whatever are the coordinates of the center of the sample according to X and Y . If we have a disordered system and are sweeping in energy, then we may set $\lambda_3 = E_F$ to a value where the localizer is, according to the computer, singular. Technically, we should not calculate the index there, but it is often simpler to treat 0 as positive when counting eigenvalues. This happens so infrequently as to be a negligible effect. (This is a guess. In fact, the author knows of no study on the accuracy of calculating the the signature of large, sparse Hermitian matrices. Most related work in numerical linear algebra is on estimating the number of eigenvalues in a region [20], which is of no use in the context of numerical K -theory.)

In theory, we can avoid computing the pseudospectrum for a study of disorder averaged index. However, we need a way to set κ , and looking at the pseudospectrum is one way to figure values for κ . The theory of how to set κ is the subject of continuing research [27].

Some may complain that if we need to tune the localizer index to use it, then it is not useful. However, many measurement instruments need tuning. In particular, when using a scanning tunneling microscope (STM) to do spectroscopy, one must determine the sample to tip gap. Let us focus on $E_F = 0$ and “probing” at the center of the sample, so $\mathbf{\lambda} = \mathbf{0}$. For simplicity, let us assume there is no lattice point at $(0, 0)$. If κ is very small the localizer index is zero because then

$$L_{\mathbf{0}}(\kappa X, \kappa Y, H) = \begin{bmatrix} H & \kappa X - i\kappa Y \\ \kappa X + i\kappa Y & -H \end{bmatrix} \approx \begin{bmatrix} H & 0 \\ 0 & -H \end{bmatrix}$$

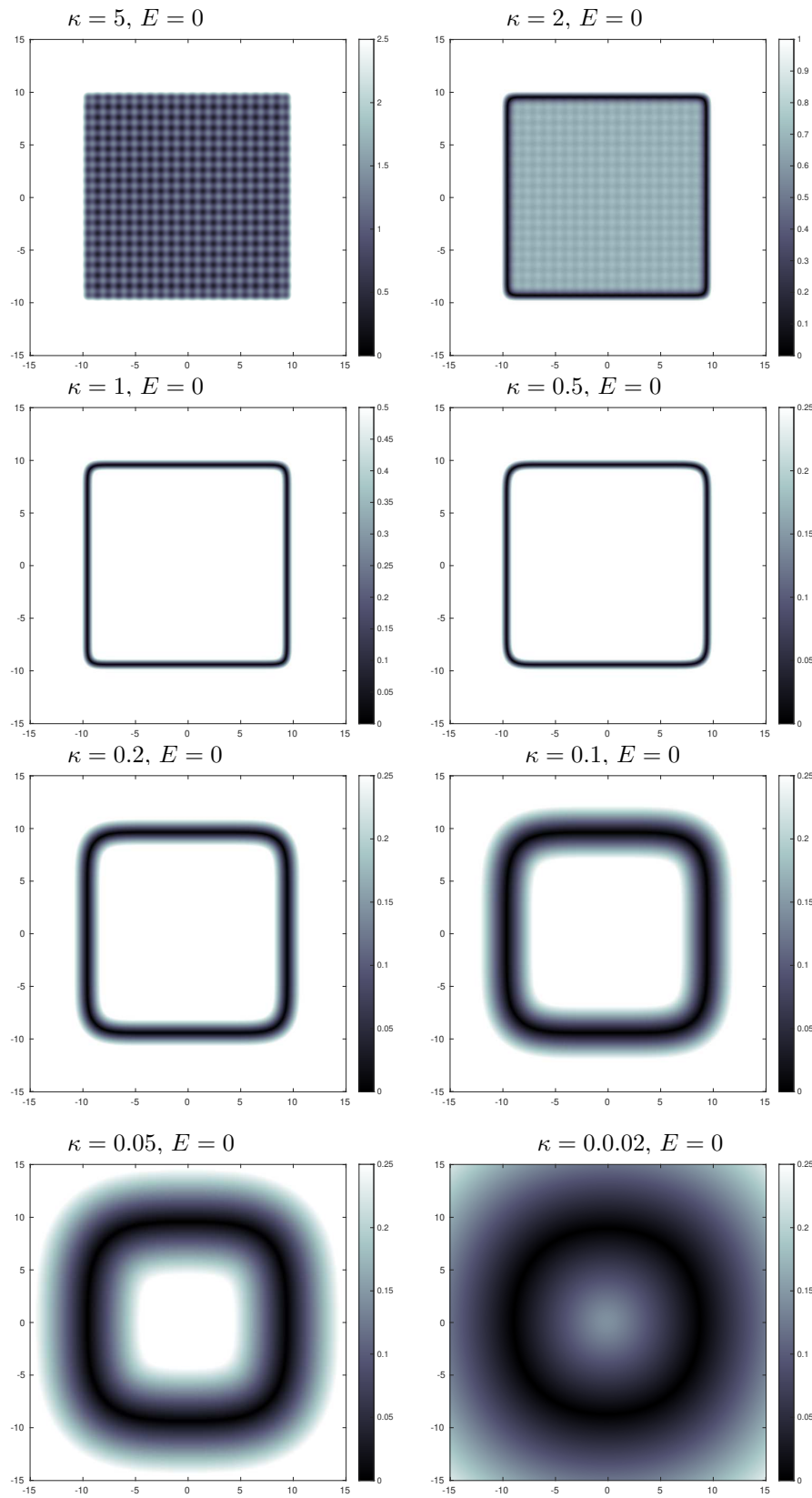


FIGURE 5.2. A slice of the pseudospectrum at $\lambda_3 = E_F = 0$. No disorder, various κ .

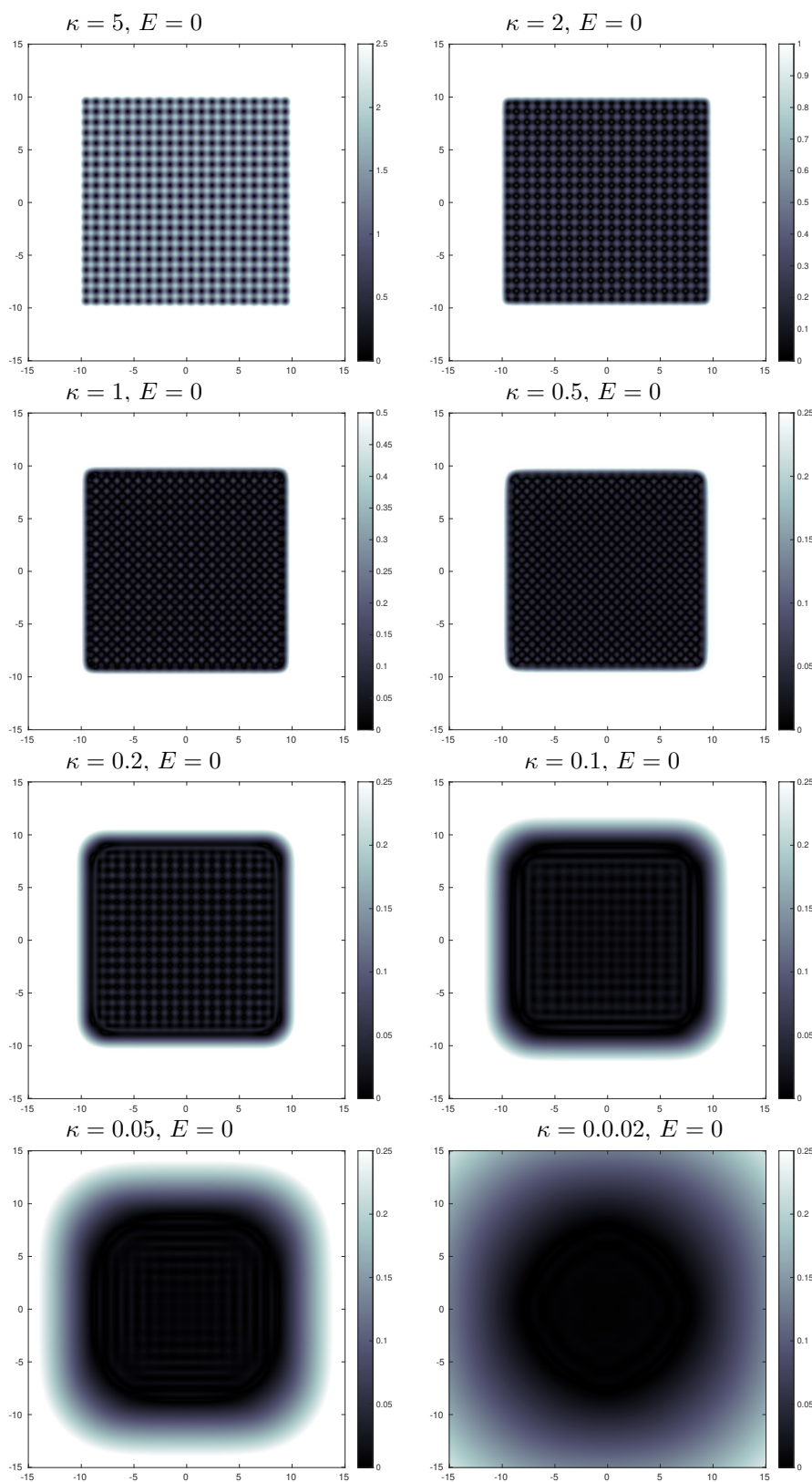


FIGURE 5.3. A slice of the pseudospectrum at $\lambda_3 = E_F = -2.4$. No disorder, various κ .

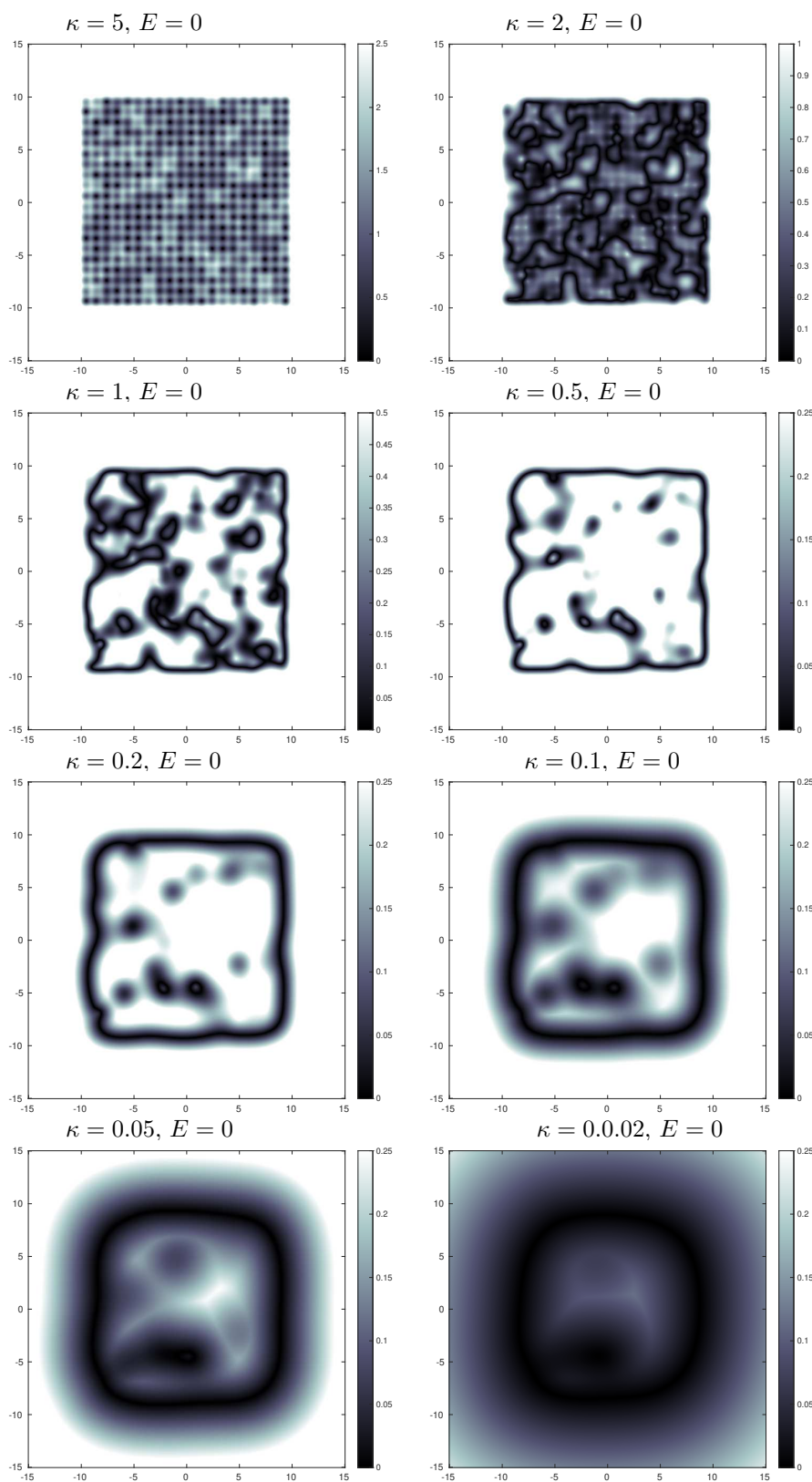


FIGURE 5.4. A slice of the pseudospectrum at $\lambda_3 = E_F = 0$. Strong disorder, various κ .

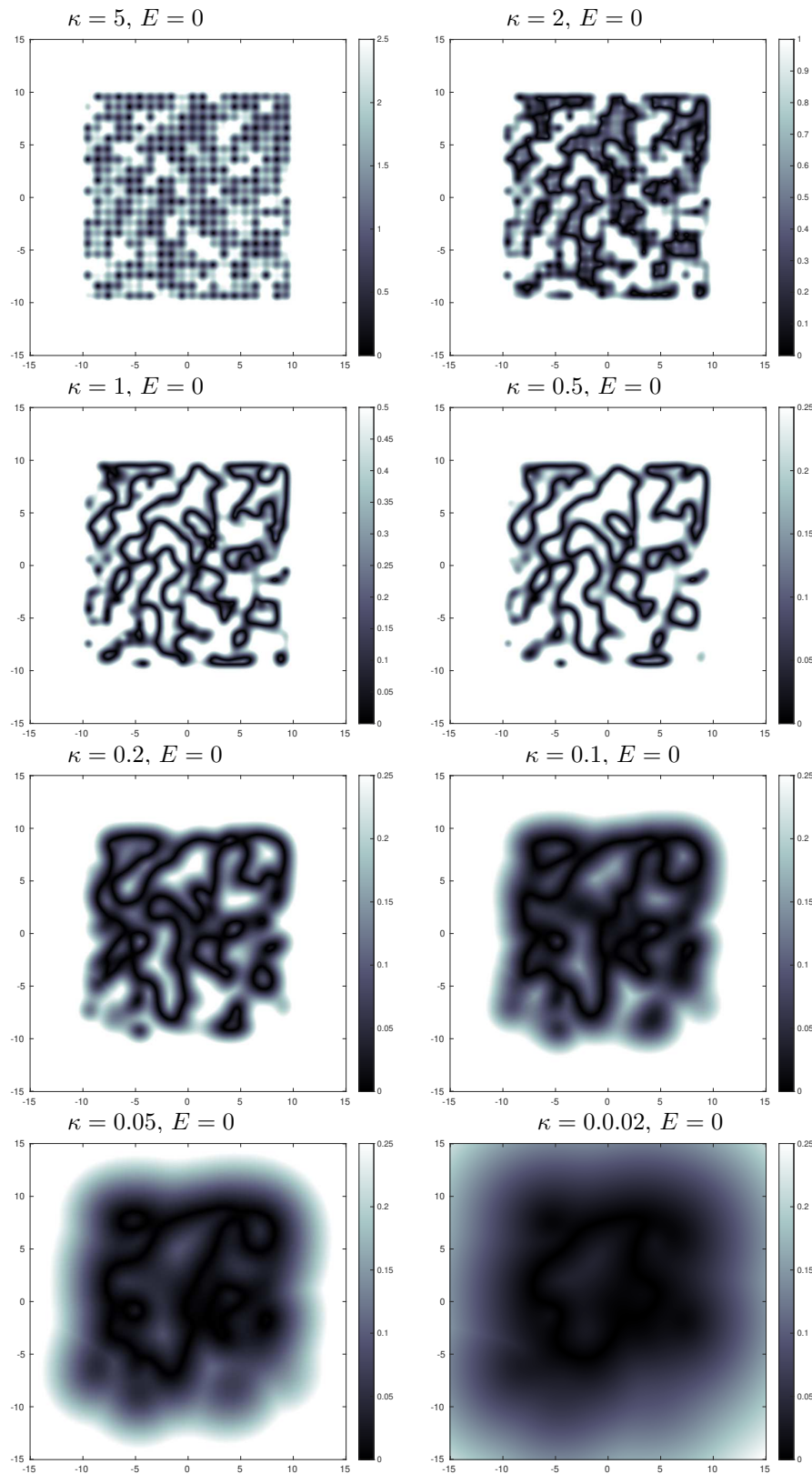


FIGURE 5.5. A slice of the pseudospectrum at $\lambda_3 = E_F = -2.4$. Strong disorder, various κ .

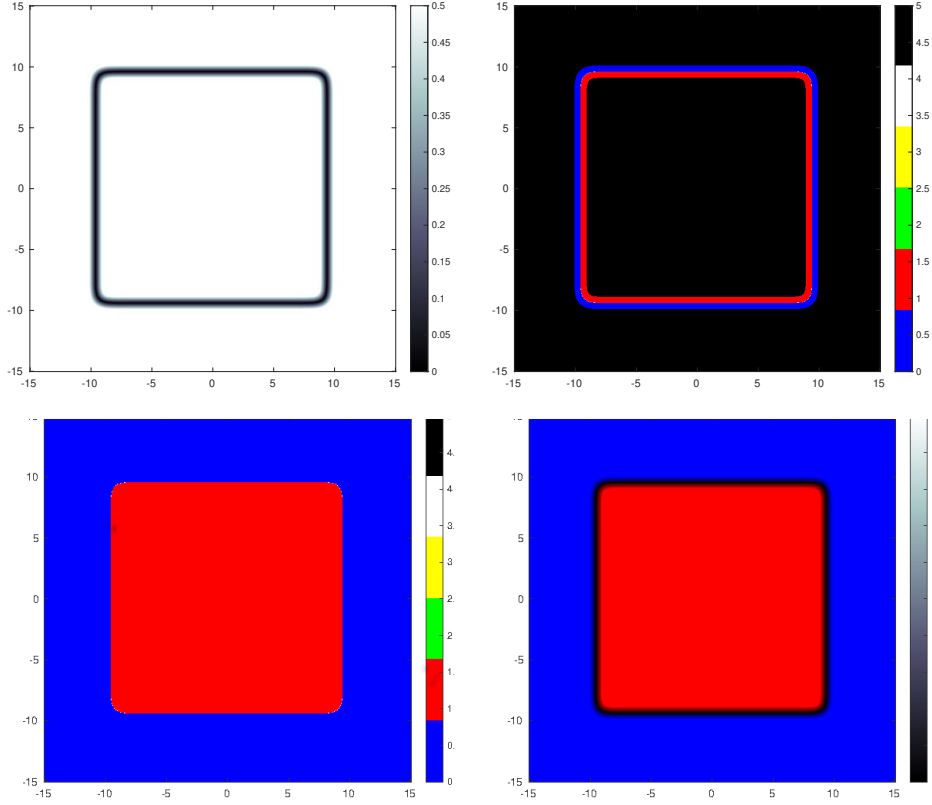


FIGURE 5.6. Pseudospectrum. Computed index. Extended by using image editing software. Index overlaid (darken only mode) on pseudospectrum. Blue is index 0. Red is index 1. Total black is where the Clifford spectrum and points where localizer gap is too small for the index to make even a little sense.

and the matrix on the right has spectrum that is symmetric across 0. Also the localizer index is zero if κ is large because then

$$L_0(\kappa X, \kappa Y, H) = \begin{bmatrix} H & \kappa X - i\kappa Y \\ \kappa X + i\kappa Y & -H \end{bmatrix} \approx \kappa \begin{bmatrix} 0 & X - iY \\ X + iY & 0 \end{bmatrix}$$

and, since $X + iY$ is normal we again find spectrum that is symmetric across 0.

Finding the intermediate values of κ that work can be done in several ways. One way is to look at the joint approximate eigenvectors [24, Lemma 1.2] for X , Y and H that can be extracted from the localizer, comparing the deviation of that state in position to system size and the deviation of that state in energy compared to the predicted bulk gap. Here we take a more visual approach.

First we look at a slice of the pseudospectrum at two energy levels, across a small sample, shown in Figures 5.2 and 5.3. We see that for large κ , the image looks somewhat like STM microscopy imagery, just showing us where the lattice points are. That is, H is almost completely ignored. For small κ , it is the position information that is getting ignored. What we are looking for is a clear distinction between edge effects at $E_F = 0$ and bulk effects at $E_F = -2.4$. This is all done with the Hamiltonian used in Section 4, and with $L = 20$. Looking at Figures 5.2 and 5.3 we might think $0.05 \leq \kappa \leq 1$ can work.

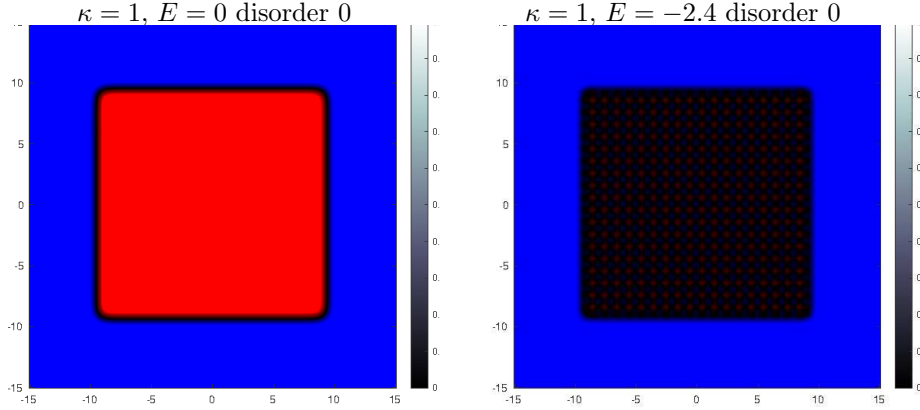


FIGURE 5.7. Index as color overlay on pseudospectrum, no disorder, at $\lambda_3 = E_F = 0$ and $\lambda_3 = E_F = -2.4$.

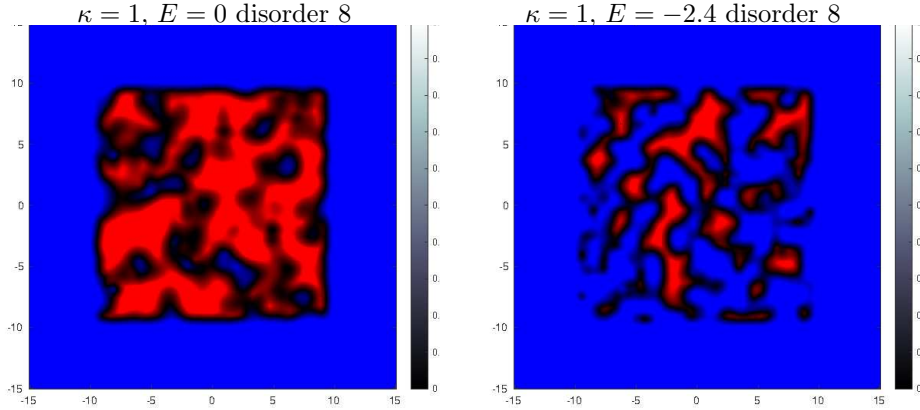


FIGURE 5.8. Index as color overlay on pseudospectrum, with disorder, at $\lambda_3 = E_F = 0$ and $\lambda_3 = E_F = -2.4$.

We also want a stability against disorder. With the rather strong disorder as used in Section 4, and just one sample, the same slices are shown in Figures 5.4 and 5.5. At $E_F = 0$, as shown in Figure 5.4, we see still a clear boundary and lots of area inside the boundary which it is safe to assume has index 0 where defined, at least for $0.1 \leq \kappa \leq 1$. The data in Figure 5.5 is harder to interpret without the K -theory data. What we expect, based on the average Bott index study as in Figure 4.1, is that the slice at $E_F = -2.4$ with this level of disorder should have, approximately by area, equal parts index 0 and index 1.

Computing multivariate pseudospectrum has not caught the attention of numerical analysts. The method the author has developed is rather crude. It does have one optimization, which is that when a large gap (meaning

$$\text{gap}_\lambda(M_1, M_2, M_3) = \|(L_\lambda(\kappa X, \kappa Y, H))^{-1}\|^{-1}$$

or the smallest absolute value of an eigenvalue of the localizer) is found, there is no need to compute the gap a near locations. This is based on [24, Lemma 7.2]. In regions where the gap stays enough above zero (say 10^{-8}) where we can trust the numerical calculations, the index cannot change. As such, well-optimized software would first compute the pseudospectrum, ignoring regions where the gap is large, then compute the contiguous gapped regions, then

compute the index at one point in each region. For now, we don't have such an optimization, and compute the index everywhere where the gap is neither too small to be meaningful or too large to be necessary. One hopes an applied mathematician will find this of interest in the near future.

The index data computed is as shown in the top-left panel of Figure 5.6. The author shamelessly used image processing software to extend the index data to contiguous regions and then used a darkening-only overlay of the index color data over the pseudospectrum. Regions that are too dark to distinguish hue are where the local index is nearly meaningless. It is differing index in locations with a decent gap that are of interest, following the logic of [24, Lemma 7.5]. This seems like a good way to visualize the index and pseudospectrum together.

Recall that the pseudospectrum is a grey scale map on three space, and it is regions of 3-space we should be coloring. Producing and displaying such information is difficult to do with current algorithms. An attempt to display the full Clifford pseudospectrum was made in Figures 2.1 and 2.2, and one sees the large interior space, in the shape of a distorted cube in Figure 2.1 and a distorted solid torus in Figure 2.2, where the index is nonzero. There seem to be smaller regions that most likely have nonzero index at higher and lower energies, but marking this by index will be difficult to even display.

For now, we are just trying explain what are good values of κ for systems here of $L = 20$. Figure 5.7 shows the index data with the pseudospectral data for $\kappa = 1$ and a clean system. Figure 5.8 shows the same but now with disorder, showing "in the bulk" mainly index 1 at $E_F = 0$ and a blend of index 0 and index 1 at $E_F = -2.4$.

The fact that the left panel of Figure 5.8 shows some index 0 well in from the edge indicates a difficulty we have in dealing with open boundaries. Changing κ does not make this go away. What works is moving to a larger system, say $L = 60$. This is above where we can easily make pictures. What was advocated in [24] was to keep κ constant as L increases to create a local invariant, and to set $\kappa = C/L$ for some fixed C to create a global index. Setting $\kappa = C/L$ may well work in a gapped system. It seems that when dealing with a mobility gap the situation can be more subtle.

6. LOCALIZER INDEX GOES GLOBAL

We start with doing the disorder average study with $L = 20, 40, 60, 80$ using the localizer index, setting $\kappa = C/L$. We have an idea, based on setting κ for $L = 20$, that we want $0.1 \leq \frac{C}{20} \leq 1$ and so $2 \leq C \leq 20$. Unfortunately, various values in and around C fail to lead to convincing results, as shown in Figure 6.1. None of these look at all like Figure 4.1.

Looking at the plots in Figure 6.2, and many others, it seemed the steeper plots correspond to smaller κ , but not for all L . So perhaps it is $\kappa \rightarrow 0$ here that plays the role of $L \rightarrow \infty$ when working with the Bott index. Various calculations, for example in [25, 27], tell us that the localizer gap often converges when $L \rightarrow \infty$. See Lemma 7.1.

Figure 6.2 shows what happens for various values of κ , computing the disorder averaged localizer index at a range of Fermi levels, as L increase somewhat. We emphasize that we stick with $\lambda_1 = \lambda_2 = 0$ unless we have a good reason, like a hole in our system, so that is the one choice we make in this section and the last. These are too computationally intensive to extend much further, but we have soft evidence that these plots have essentially converged at the higher values for L shown in each instance.

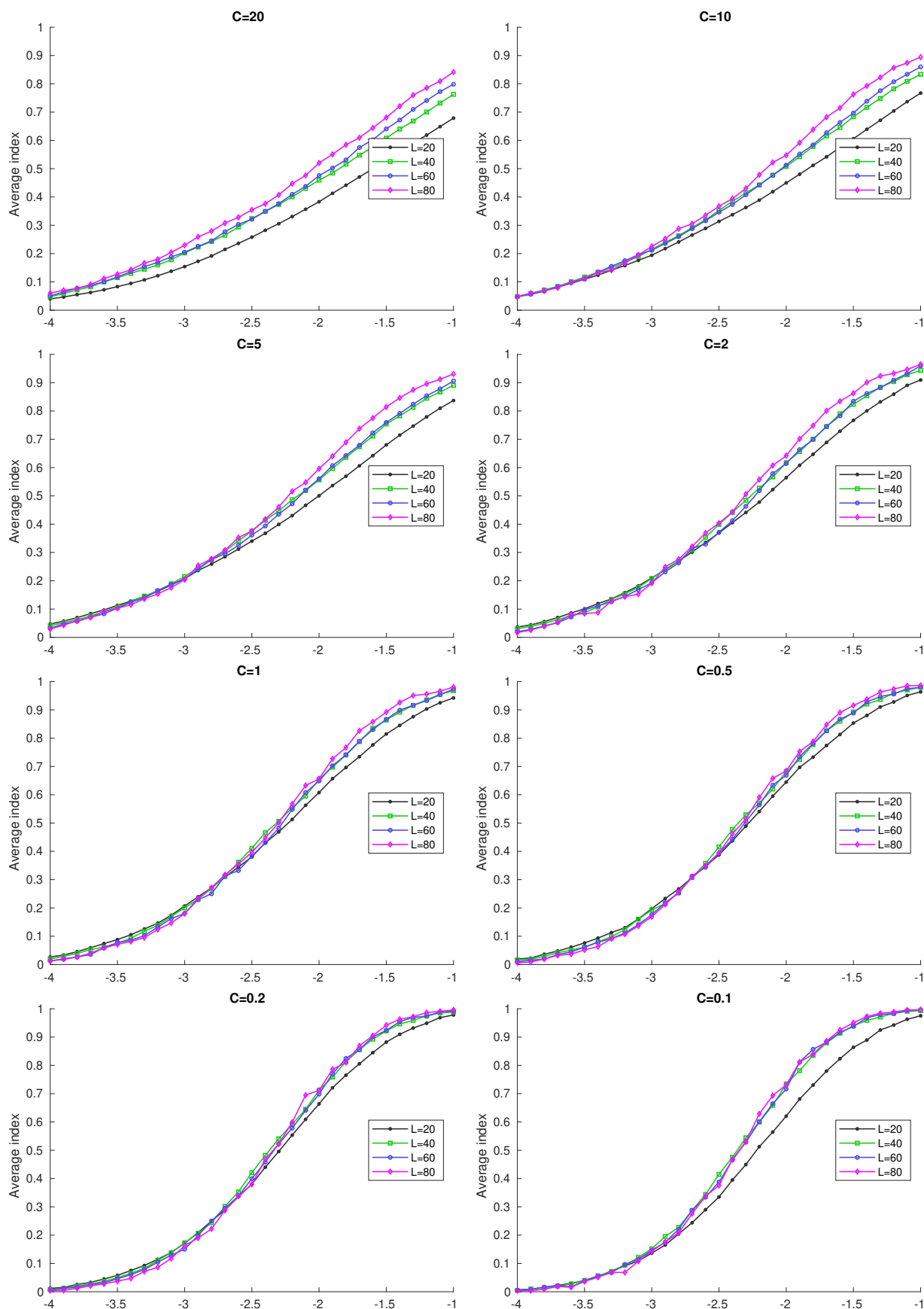


FIGURE 6.1. Disorder averaged localizer index, with $\kappa = C/L$.

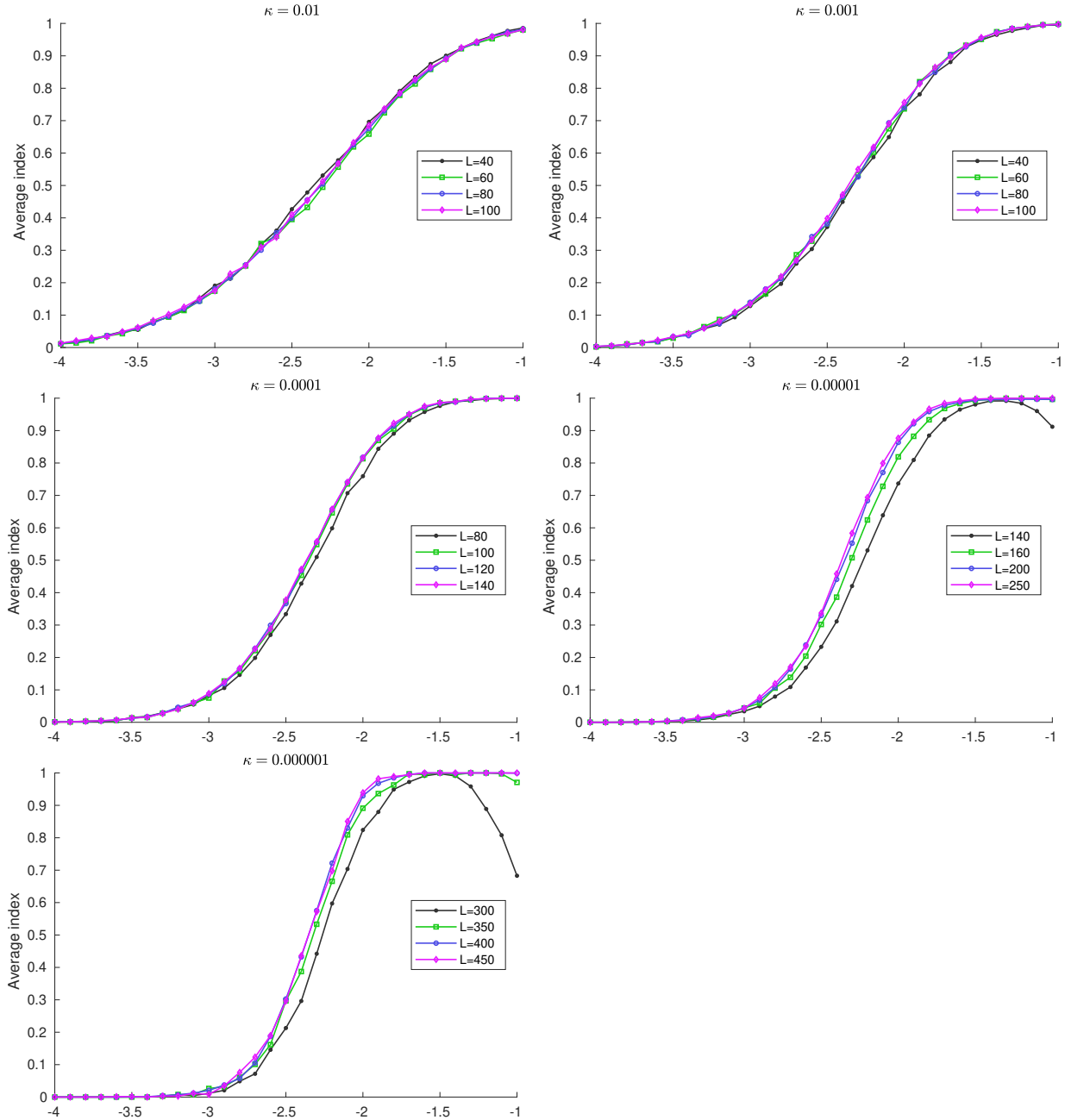


FIGURE 6.2. Various κ values, searching for appropriate value for L .

There is some theory when one has a bulk gap of a known size, as in [21]. However, we have just a mobility gap. Presumably, one could work in an appropriate C^* -algebra, find a gapped Hamiltonian that lives in that C^* -algebra and can extend the methods of [21] to that setting. For now, we are happy to gather numerical evidence.

In Figure 6.3 shows the plots for various decreasing κ . Notice they are decreasing by powers of ten. The plots in Figure 6.2 were used to deduce a reasonable values of L to go with each value of κ . It is perhaps the case that open boundaries really interact with disorder and this is what forced us into such large systems to see plots to create Figure 6.3.

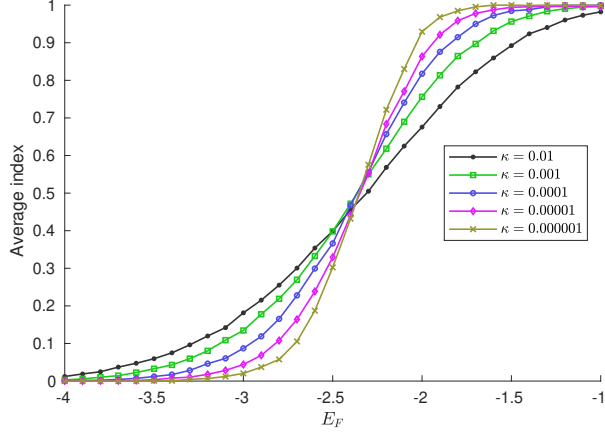


FIGURE 6.3. Localizer index averaged over disorder as a function of the Fermi level: $\kappa = 0.01$ (16,955 samples with $L=80$); $\kappa = 0.001$ (14,878 samples with $L=100$); $\kappa = 0.0001$ (5,598 samples with $L=120$); $\kappa = 0.00001$ (8,031 samples with $L=200$); $\kappa = 0.000001$ (870 samples with $L=400$).

7. LOCAL NATURE OF THE LOCALIZER

Better algorithms are needed to make the spectral localizer effective for three-dimensional systems, and indeed would help with two-dimensional systems. Here is one possible improvement.

Suppose one is working on a two-dimensional system with $L \geq 300$ for a specific λ . It should be possible to compute the gap and index of a further truncation of the system to smaller size and use those results if that gap is large enough, and only if this is small recomputing the gap and index on the full system. This should be possible due to the local nature of the localizer, where drastic alterations of the Hamiltonian away from the (λ_1, λ_2) have little effect, as we will soon see. Also, it is the smaller values of the localizer gap that need to be computed precisely.

A glance of Figures 2.1 and 2.2 shows that, at least in one instance, something drastic like cutting out a hole in the middle of a sample has little effect on the pseudospectrum at the edge. An analytic expression of this fact is the following lemma. This was proving jointly with Schulz-Baldes years ago, but in this form it never found a place in our papers. Many similar, and more technical results, are in our papers [27, 28, 21].

For simplicity, we state this regarding computing the spectral gap for the localizer when $\lambda = \mathbf{0}$, and only for three matrices (so two physical dimensions). So let $L = L_0$. Notice also the lemma is stated in terms of changes to the square of the localizer gap.

Lemma 7.1. *Suppose X, Y and H are Hermitian matrices, with X and Y commuting, and set*

$$\gamma = \|L(X, Y, H)^{-1}\|^{-2}.$$

Let $Z = X + iY$. If H_0 is Hermitian with

$$(7.1) \quad \||Z|^{-1} (HH_0 + H_0H + H_0^2) |Z|^{-1}\| \leq C$$

and

$$\|[Z, H]\| \leq D$$

and

$$(7.2) \quad \left\| |Z|^{-1} [Z, H_0] |Z|^{-1} \right\| \leq E$$

then

$$|\gamma - \gamma_0| \leq (C + E) \gamma + (C + E) D$$

where

$$\gamma_0 = \left\| L(X, Y, H + H_0)^{-1} \right\|^{-2}.$$

If

$$\gamma > \frac{(C + E)D}{1 - (C + E)}$$

then the index at zero for $(X, Y, H + H_0)$ will be the same as for (X, Y, H) .

Proof. Notice Z is normal, and compute:

$$L(X, Y, H) = \begin{bmatrix} H & Z^\dagger \\ Z & -H \end{bmatrix},$$

$$L(X, Y, H)^2 = \begin{bmatrix} H^2 + |Z|^2 & -[H, Z]^\dagger \\ -[H, Z] & H^2 + |Z|^2 \end{bmatrix},$$

$$L(X, Y, H + H_0)^2 = L(X, Y, H)^2 + \begin{bmatrix} HH_0 + H_0H + H_0^2 & -[H_0, Z]^\dagger \\ -[H_0, Z] & HH_0 + H_0H + H_0^2 \end{bmatrix}.$$

We deduce from (7.1) that

$$-C|Z|^2 \leq HH_0 + H_0H + H_0^2 \leq C|Z|^2.$$

From (7.2) we deduce

$$\begin{bmatrix} -E|Z| & 0 \\ 0 & -E|Z| \end{bmatrix} \leq \begin{bmatrix} 0 & -[H_0, Z]^* \\ -[H_0, Z] & 0 \end{bmatrix} \leq \begin{bmatrix} E|Z| & 0 \\ 0 & E|Z| \end{bmatrix}.$$

We find

$$\begin{aligned} & L(X, Y, H + H_0)^2 \\ &= \begin{bmatrix} H^2 + |Z|^2 & -[H, Z]^* \\ -[H, Z] & H^2 + |Z|^2 \end{bmatrix} + \begin{bmatrix} HH_0 + H_0H + H_0^2 & -[H_0, Z]^* \\ -[H_0, Z] & HH_0 + H_0H + H_0^2 \end{bmatrix} \\ &\geq \begin{bmatrix} (1 - C - E)H^2 + |Z|^2 & -[H, Z]^* \\ -[H, Z] & (1 - C - E)H^2 + |Z|^2 \end{bmatrix} + \begin{bmatrix} (-C - E)|Z|^2 & 0 \\ 0 & (-C - E)|Z|^2 \end{bmatrix} \\ &= (1 - C - E)B(X, Y, H)^2 + \begin{bmatrix} 0 & (C + E)[H, Z]^* \\ (C + E)[H, Z] & 0 \end{bmatrix} \\ &\geq (1 - C - E)B(X, Y, H)^2 - (C + E)D \end{aligned}$$

and

$$\begin{aligned}
& L(X, Y, H + H_0)^2 \\
&= \begin{bmatrix} H^2 + |Z|^2 & -[H, Z]^* \\ -[H, Z] & H^2 + |Z|^2 \end{bmatrix} + \begin{bmatrix} HH_0 + H_0H + H_0^2 & -[H_0, Z]^* \\ -[H_0, Z] & HH_0 + H_0H + H_0^2 \end{bmatrix} \\
&\leq \begin{bmatrix} (1 + C + E)H^2 + |Z|^2 & -[H, Z]^* \\ -[H, Z] & (1 + C + E)H^2 + |Z|^2 \end{bmatrix} + \begin{bmatrix} (C + E)|Z|^2 & 0 \\ 0 & (C + E)|Z|^2 \end{bmatrix} \\
&= (1 + C + E)B(X, Y, H)^2 + \begin{bmatrix} 0 & (-C - E)[H, Z]^* \\ (-C - E)[H, Z] & 0 \end{bmatrix} \\
&\leq (1 + C)B(X, Y, H)^2 + (C + E)D.
\end{aligned}$$

□

ACKNOWLEDGMENTS

This material is based upon work supported by the National Science Foundation under DMS 1700102. The author thanks Liang Du for pointing out the differing use of the constants in the BHZ model. Most of the computing was done on machines at the Center for Advance Research Computing at the University of New Mexico. The author is most grateful to Hermann Schulz-Baldes for allowing Lemma 7.1 to appear here.

REFERENCES

- [1] Matlab function ldl documentation. mathworks.com/help/matlab/ref/ldl.html. Accessed: 2019-07-24.
- [2] MUltifrontal Massively Parallel Solver Users guide. mumps.enseeiht.fr/doc/userguide_5.2.1.pdf. Accessed: 2019-07-24.
- [3] Supplementary files. math.unm.edu/%7Eloring/BottLocalizerGuide/.
- [4] Miguel A Bandres, Mikael C Rechtsman, and Mordechai Segev. Topological photonic quasicrystals: Fractal topological spectrum and protected transport. *Physical Review X*, 6(1):011016, 2016.
- [5] J. Bellissard, A. van Elst, and H. Schulz-Baldes. The noncommutative geometry of the quantum Hall effect. *J. Math. Phys.*, 35(10):5373–5451, 1994. Topology and physics.
- [6] Michele Benzi, Paola Boito, and Nader Razouk. Decay properties of spectral projectors with applications to electronic structure. *SIAM review*, 55(1):3–64, 2013.
- [7] David Berenstein and Eric Dzienkowski. Matrix embeddings on flat \mathbb{R}^3 and the geometry of membranes. *Physical Review D*, 86(8):086001, 2012.
- [8] Raffaello Bianco and Raffaele Resta. Mapping topological order in coordinate space. *Physical Review B*, 84(24):241106, 2011.
- [9] Bruce Blackadar. Shape theory for C^* -algebras. *Math. Scand.*, 56(2):249–275, 1985.
- [10] Alain Connes and Nigel Higson. Déformations, morphismes asymptotiques et K -théorie bivariante. *C. R. Acad. Sci. Paris Sér. I Math.*, 311(2):101–106, 1990.
- [11] Luca D’Alessio and Marcos Rigol. Dynamical preparation of Floquet Chern insulators. *Nature communications*, 6:8336, 2015.
- [12] Søren Eilers and Terry A. Loring. Computing contingencies for stable relations. *Internat. J. Math.*, 10(3):301–326, 1999.
- [13] Søren Eilers, Terry A. Loring, and Gert K. Pedersen. Morphisms of extensions of C^* -algebras: pushing forward the Busby invariant. *Adv. Math.*, 147(1):74–109, 1999.
- [14] Ruy Exel and Terry A. Loring. Invariants of almost commuting unitaries. *J. Funct. Anal.*, 95(2):364–376, 1991.
- [15] Ion C Fulga, Dmitry I Pikulin, and Terry A Loring. Aperiodic weak topological superconductors. *Physical review letters*, 116(25):257002, 2016.
- [16] Matthew B. Hastings and Terry A. Loring. Topological insulators and C^* -algebras: Theory and numerical practice. *Ann. Physics*, 326(7):1699–1759, 2011.

- [17] Hua Jiang, Lei Wang, Qing-feng Sun, and XC Xie. Numerical study of the topological anderson insulator in HgTe/CdTe quantum wells. *Physical Review B*, 80(16):165316, 2009.
- [18] Vladimir Kisil. Möbius transformations and monogenic functional calculus. *Electron. Res. Announc. Math. Sci*, 2(1):26–33, 1996.
- [19] Alexei Kitaev. Anyons in an exactly solved model and beyond. *Annals of Physics*, 321(1):2–111, 2006.
- [20] Lin Lin, Yousef Saad, and Chao Yang. Approximating spectral densities of large matrices. *SIAM review*, 58(1):34–65, 2016.
- [21] Terry Loring and Hermann Schulz-Baldes. The spectral localizer for even index pairings. *J. Noncommut. Geom.*, to appear. arXiv preprint arXiv:1802.04517.
- [22] Terry A. Loring. K -theory and asymptotically commuting matrices. *Canad. J. Math.*, 40(1):197–216, 1988.
- [23] Terry A. Loring. C^* -algebra relations. *Math. Scand.*, 107(1):43–72, 2010.
- [24] Terry A. Loring. K -theory and pseudospectra for topological insulators. *Ann. Physics*, 356:383–416, 2015.
- [25] Terry A Loring. Bulk spectrum and k -theory for infinite-area topological quasicrystal. *arXiv preprint arXiv:1811.07494*, 2018.
- [26] Terry A. Loring and Matthew B. Hastings. Disordered topological insulators via C^* -algebras. *Europhys. Lett. EPL*, 92:67004, 2010.
- [27] Terry A. Loring and Hermann Schulz-Baldes. Finite volume calculation of K -theory invariants. *New York J. Math.*, 23:1111–1140, 2017.
- [28] Terry A Loring and Hermann Schulz-Baldes. Spectral flow argument localizing an odd index pairing. *Canadian Mathematical Bulletin*, 62(2):373–381, 2019.
- [29] Noah P Mitchell, Lisa M Nash, Daniel Hexner, Ari M Turner, and William TM Irvine. Amorphous topological insulators constructed from random point sets. *Nature Physics*, 14(4):380, 2018.
- [30] Emil Prodan. Disordered topological insulators: a non-commutative geometry perspective. *J. Phys. A*, 44(11):113001, 50, 2011.
- [31] Andreas Sykora. The fuzzy space construction kit. *arXiv preprint arXiv:1610.01504*, 2016.
- [32] Daniele Toniolo. Time-dependent topological systems: A study of the bott index. *Physical Review B*, 98(23):235425, 2018.
- [33] Jonas; Viesca, Edgar Lozano; Schober and Hermann Schulz-Baldes. Chern numbers as half-signature of the spectral localizer. *J. Math. Phys.*, to appear.

DEPARTMENT OF MATHEMATICS AND STATISTICS, UNIVERSITY OF NEW MEXICO, ALBUQUERQUE, NEW MEXICO 87131, USA

E-mail address: loring@math.unm.edu